Molybdenum nanopillar arrays
Fabrication and engineering

Maduro, Louis; de Boer, Charles; Zuiddam, Marc; Memisevic, Elvedin; Conesa-Boj, Sonia

DOI
10.1016/j.physe.2021.114903

Publication date
2021

Document Version
Final published version

Published in
Physica E: Low-Dimensional Systems and Nanostructures

Physica E 134 (2021) 114903

Contents lists available at ScienceDirect

Physica E: Low-dimensional Systems and Nanostructures

journal homepage: www.elsevier.com/locate/physe

Molybdenum nanopillar arrays: Fabrication and engineering

Louis Maduro, Charles de Boer, Marc Zuiddam, Elvedin Memisevic, Sonia Conesa-Boj *

Kavli Institute of Nanoscience, Delft University of Technology, 2628CJ, Delft, the Netherlands

ARTICLE INFO

Keywords:
Molybdenum
Nanopillars
Cryogenic etching
Shape control
Hydrogen silsesquioxane negative resist

ABSTRACT

We report on the fabrication of molybdenum (Mo) nanopillar (NP) arrays with NP diameters down to 75 nm by means of deep-reactive ion etching at cryogenic temperatures. A variable-thickness Mo metal layer sputtered onto a Si_3N_4/Si substrate makes possible NPs with different lengths in a controllable manner. We demonstrate how our fabrication strategy leads to tunable cross-sections with different geometries, including hexagonal, cylindrical, square and triangular shapes, by using electron beam lithography on hydrogen silsesquioxane negative tone resist. To ensure well-defined facets and surfaces, we employ deep-reactive ion etching in a gas mixture of SF_6 and O_2 at cryogenic temperatures in an inductively coupled plasma reactive ion etching (ICP-RIE) system. These results represent an attractive route towards the realization of high-density Mo NP arrays for applications from nanoelectronics to quantum sensing and hydrogen evolution reaction catalysis.

1. Introduction

One-dimensional (1D) Molybdenum (Mo) nanostructures have garnered significant attention recently due to their potential uses in a wealth of applications from interconnects in nanoelectronic devices to promoting the hydrogen evolution reaction [1–6]. This potential stems from their remarkable properties, such as efficient electron emission and structural stability.

Of particular interest for applications in nanoelectronics is the fact that 1D Mo nanostructures exhibit reduced resistivity with decreasing its diameter [1], thus making 1D Mo nanostructures promising candidates for interconnects for nanodevices. Furthermore, arranging 1D Mo nanostructures into geometric arrays whose axis is perpendicular to the substrate surface represents one of the main challenges for concerning their integration into nanoelectronic applications.

Previous works have extensively studied the bottom-up fabrication of 1D Mo nanostructures, focusing mostly on approaches such as electrodeposition and reduction, hydrogenation, and chemical vapour deposition [1,3–7]. However, these approaches have some limitations in terms of scalability as well as concerning the control on the orientation, shape, and density of the 1D nanostructures at spatially well-defined locations.

With this motivation, the main goal of this work is to bridge this gap by demonstrating a novel top-down approach for the large-scale fabrication of 1D Mo nanostructures, denoted in the following as nanopillars (NPs), arrays whose shape, diameter, pitch, and length can be fully controlled by deploying a combination of sputter-deposition, electron beam lithography, and cryogenic deep-reactive ion etching techniques.

Our strategy for the large-scale fabrication of Mo NPs draws inspiration from the cryogenic deep-reactive ion etching of silicon, where micron-depth smooth vertical sidewalls can be formed when using SF_6/O_2 gas mixture [8–12].

The close similarity between the etching processes of refractory metals and of Si suggests that a cryogenic deep-reactive ion etching process could be adopted to fabricate nanostructures with well-defined sidewalls also in the case of Mo.

With this motivation, in this work we modify the electron beam lithography and cryogenic deep-reactive ion etching procedure for Si nanopillar fabrication [13–16] to fabricate Mo NPs. We believe that these results would enable a wide range of technological applications.

2. Molybdenum nanopillar array fabrication

Our fabrication strategy is schematically displayed in Fig. 1. Pieces of 1×1 cm^2 p-doped Si(001) are used throughout the whole process. Firstly, the Si pieces are cleaned via the RCA process [17]. Secondly, a low-stress Si_3N_4 layer is grown on top of the silicon pieces by means of low-pressure chemical vapour deposition (LPCVD) in a Tempress furnace. The Si_3N_4 layer is used as a protective layer for the Si pieces, since it is well-known that Si is etched in SF_6/O_2 gas mixtures. Subsequently, a layer of molybdenum (Mo) is sputter-deposited on top of this Si_3N_4 layer by using an Alliance Concept Ac 450 sputter-deposition

* Corresponding author.
E-mail address: s.conesaboj@tudelft.nl (S. Conesa-Boj).

https://doi.org/10.1016/j.physe.2021.114903
Received 2 March 2021; Received in revised form 24 June 2021; Accepted 9 July 2021
Available online 13 July 2021

system with an DC power of 100 W at a pressure of 3.4 μbar. The thickness of the Mo layer used in this work is varied from 350 nm to 880 nm.

2.1. Electron-beam lithography

Afterwards, a spin coating of negative tone resist is carried out on top of the Mo metal layer. Crucially, in order to ensure the desired nanopillar dimensions, the resist mask needs to have high plasma resistance while also being able to maintain the mask shape during the etching process. To fulfill these requirements, Flowable Oxide-16 (FOx-16) and Flowable Oxide-25, (FOx-25) from Dow Corning were adopted in this work [18].

Before applying the FOx resist, a monolayer of HexaMethylDiSilazane (HMDS) adhesion promoter is evaporated on top of the metal layer using a Delta RC80 apparatus from Suss Microtech [19]. The FOx resist is left to warm up to room temperature [20] and then a spincoat speed between 1500- and 10,000 rpm is used to acquire a uniform resist layer on the samples. A resist thickness between 800 nm and 400 nm was achieved with the FOx-25 resist for the used spincoat speeds, while for the case of FOx-16 a resist thickness between 600 nm and 400 nm is achieved.

The samples are then baked on hotplates in two consecutive baking steps of 150 °C and 220 °C for 2 min each. The desired nanopillar arrays patterns are written in a RAITH 5000+ EBPG or in a RAITH 5200 EBPG system at 100 keV accelerating voltage. Proximity Effect Correction (PEC) was implemented via a Monte Carlo approach in the TRACER program from GenISys GmbH to ensure sharp edges of the smallest nanopillar patterns. The optimal dose depends both on the size of the nanopillar patterns and on the pitch-to-pitch distance between nanopillars. It is found that a larger dose is needed when decreasing the size of the nanopillar patterns and that nanopillar diameters down to 30 nm are achieved by the combination of large dose and small pitch-to-pitch nanopillar distance. After exposure, the FOx-16 was developed in 6.25% TMAH for 45 s at room temperature. In the case of FOx-25 resist, a different development procedure is required when resist layers thicker than 600 nm are used as described below.

2.2. Cryogenic deep reactive ion etching

The vertical sidewall formation in Mo NPs is achieved via cryogenic deep reactive ion etching in a SF_6/O_2 gas mixture [21–24]. We adopt this strategy since it has been already successfully applied in the case of Silicon [10,13,25–31].

Different SF_6/O_2 mixtures were considered in order to acquire the optimal etch-passivation ratio, with the most successful mixture being a gas mixture of 200.0 sccm SF_6 and 5.0 sccm O_2. A platen power of 70 W combined with an ICP power of 1100 W was used to etch the nanopillar structures. With these conditions, an etch rate of 140 nm/min is found to be suitable for the Mo structures. Subsequently, cryogenic deep-reactive ion etching of the developed samples is carried out in an Oxford Instruments PlasmaPro 100 Estrelas ICP-RIE system. The sample is placed on a carrier wafer that is clamped to a cryogenic holder cooled by a flow of liquid N_2. Helium backing is used to ensure proper thermal contact between the holder and the sample.

Before starting the etch process, a 30-min long O_2 plasma clean of the chamber is carried out at a temperature of −20 °C. The system is subsequently cooled down to the etching temperature of −100 °C (±2 °C). This etching is carried out in pulsed sequences of 100 kHz with a duty cycle of 10%. The slit-valve is left fully opened to ensure the smallest possible pressure during the etch. A 3-min pre-conditioning step of the chamber is carried out in order to guarantee reproducibility between different etching sessions [32]. Fomblin oil is placed between the sample and carrier wafer to further improve the thermal contact. After the carrier wafer with the sample is placed inside the process chamber, there needs to be a waiting time of 1 min.

After cryogenic etching the remaining FOx resist, along with the SiO_2 adhesion layer, is removed by a diluted solution of hydrofluoric acid (HF). A 5% HF dip for 120 s results in all the FOx resist and SiO_2 being removed from the nanopillar structures. We also note that the HF dip does not affect the shape of the nanopillars and barely etched away any of the underlying Si_3N_4 substrate.

3. Results and discussion

Fig. 2a displays an array of Mo nanopillars with square cross-sections, with the inset focusing on a representative NP, demonstrating that a high-yield of Mo nanopillars characterized by regular sidewalls is achieved. Fig. 2b illustrates the role played by the Si_3N_4 protective layer in the fabrication process: since the etch chemistry for Mo is presumably different from the one required for Si etching the underlying Si is etched away at a higher rate than the Mo. In turn, this higher Si etch rate leads to an undercut that results into the Mo NPs toppling onto the Si substrate.

To further demonstrate how our fabrication strategy offers precise control on the geometry of the resulting Mo NPs, equilateral triangles, circular, and hexagonal patterns are designed and the resulting Mo NP arrays are displayed in Fig. 3. The insets are top views of the respective nanopillars, highlighting the corresponding geometrical cross-sections. One can observe from Fig. 3 how Mo regular arrays of NPs with well-defined facets and varying cross-sectional shapes can be reliably fabricated for large (between 200 nm and 300 nm) nanostructures where

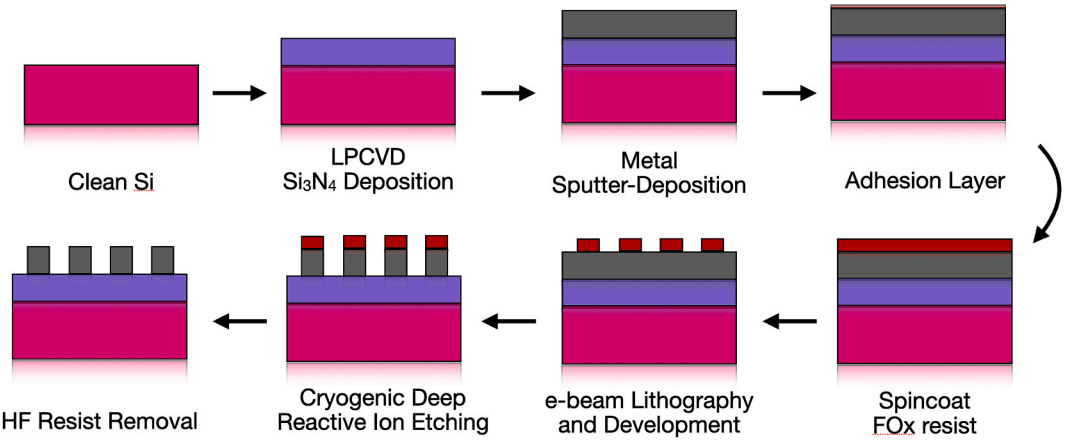

Fig. 1. Schematic of the fabrication approach of the Mo NP arrays adopted in this work. The process starts with the LPCVD deposition of the Si_3N_4 layer and ends with the HF resist removal which reveals the NP arrays.

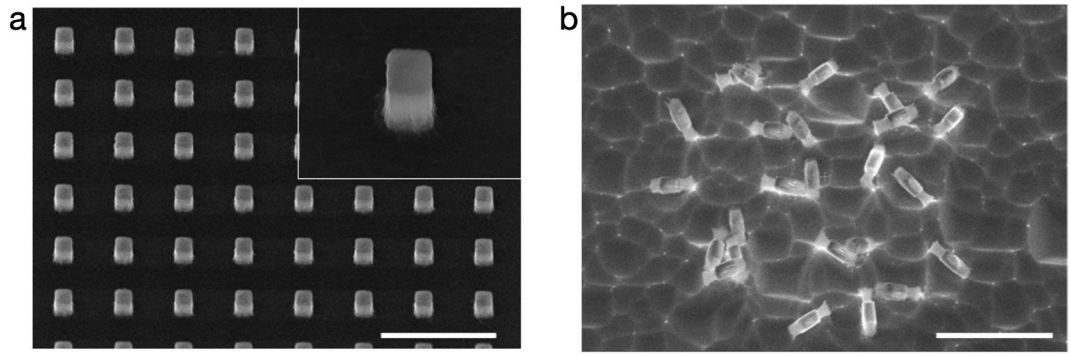

Fig. 2. SEM images of Mo nanopillars with square cross-sections fabricated on top of a Si wafer either with (a) and without (b) a protective Si_3N_4 layer, demonstrating how only in the first case a regular NP array is obtained. The inset in (a) displays a representative NP. A 350 nm layer of Mo is used for the NP fabrication. The scale bar is 2 μm.

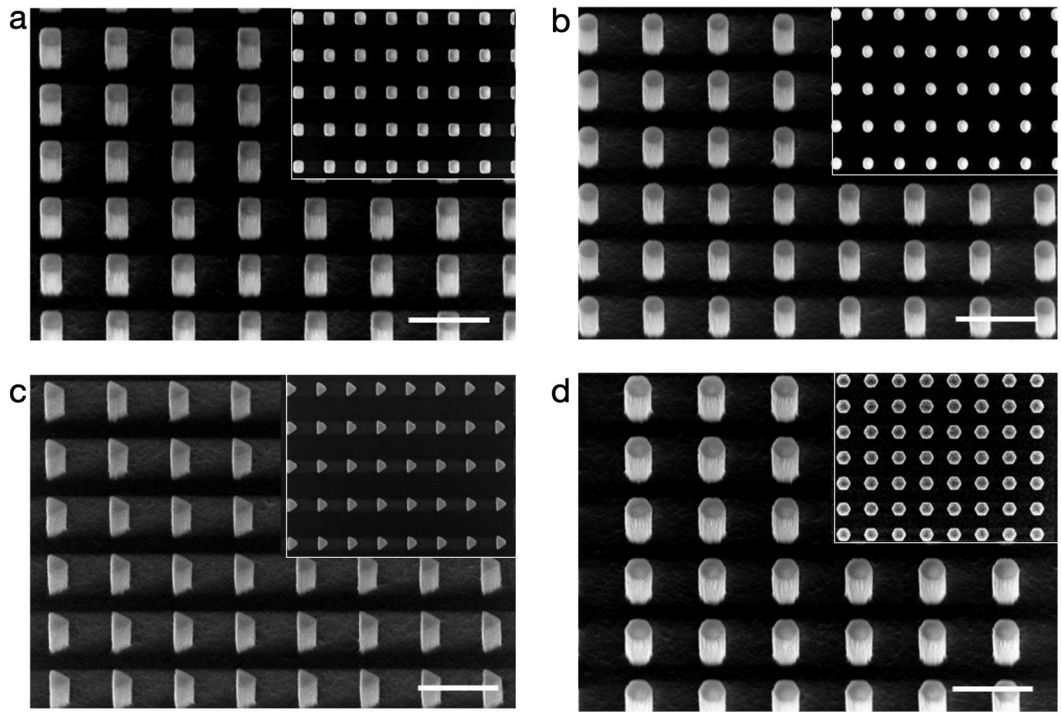

Fig. 3. SEM images of regular arrays of Mo nanopillars exhibiting (a) square, (b) circular, (c) triangular, and (d) hexagonal cross-sections respectively, as illustrated by the corresponding top-view images shown in the insets. For all the arrays a 500 nm Mo layer is used for the NP fabrication. The scale bar is 1 μm.

their shapes are retained down to the 100 nm range.

Furthermore, NP arrays with varying pitches are designed in order to determine the minimum distance achievable between the nanopillars of an array. The results for this pitch distance analysis are presented in Fig. 4. A minimum pitch distance of 300 nm was achieved in the case of NP with diameters of 100 nm. It is found that decreasing the nanopillar dimensions results in smaller pitch distances available before over-exposure results. The dosage required for the different nanopillar shapes does not vary significantly when considering the total area of each respective nanopillar, as indicated in Fig. 5.

3.1. The role of the adhesion layer: SiO_2

During the optimization process for the nanopillar array fabrication, both the FOx-16 and FOx-25 resists reached their shelf-life. One of the consequences of the aged resist is a worsening of the adhesion of the resists to the Mo surface, even when HMDS is used as an adhesion promotor. In order to recover good adhesion to the Mo surface, a SiO_2 layer is used as an alternative adhesion layer because of its close similarity to the FOx molecular structure. We note that FOx resists consist of a cage-like structure of Si–H and Si–O bonds. After exposure and development of the FOx resists, these Si–H bonds are broken and only the Si–O bonds are left [33,34]. Due to the remaining Si–O bonds in the FOx patterns, a thin layer of SiO_2 is used as an alternative to HMDS as an adhesion layer. Before applying the FOx resist, a 15 nm layer of SiO_2 on top of the Mo metal is deposited via Plasma Enhanced Chemical Vapour Deposition (PECVD) in an Oxford Instruments PlasmaPro 80 system.

After exposure, the FOx resist is developed in heated Microposit MF321 at 50 °C for 5 min, followed by a 30 s dip in H_2O. Subsequently to this H_2O dip, the samples were placed in a beaker filled with isopropanol, carefully ensuring that the surface of the substrates has always liquid on it when transferring the substrates to the different solutions mentioned above. After the development step, the samples are placed in a Leica super critical CO_2 drying system. The use of supercritical resist drying is known to be advantageous when patterning resist structures with large aspect-ratios [35–38]. We note that the combination of

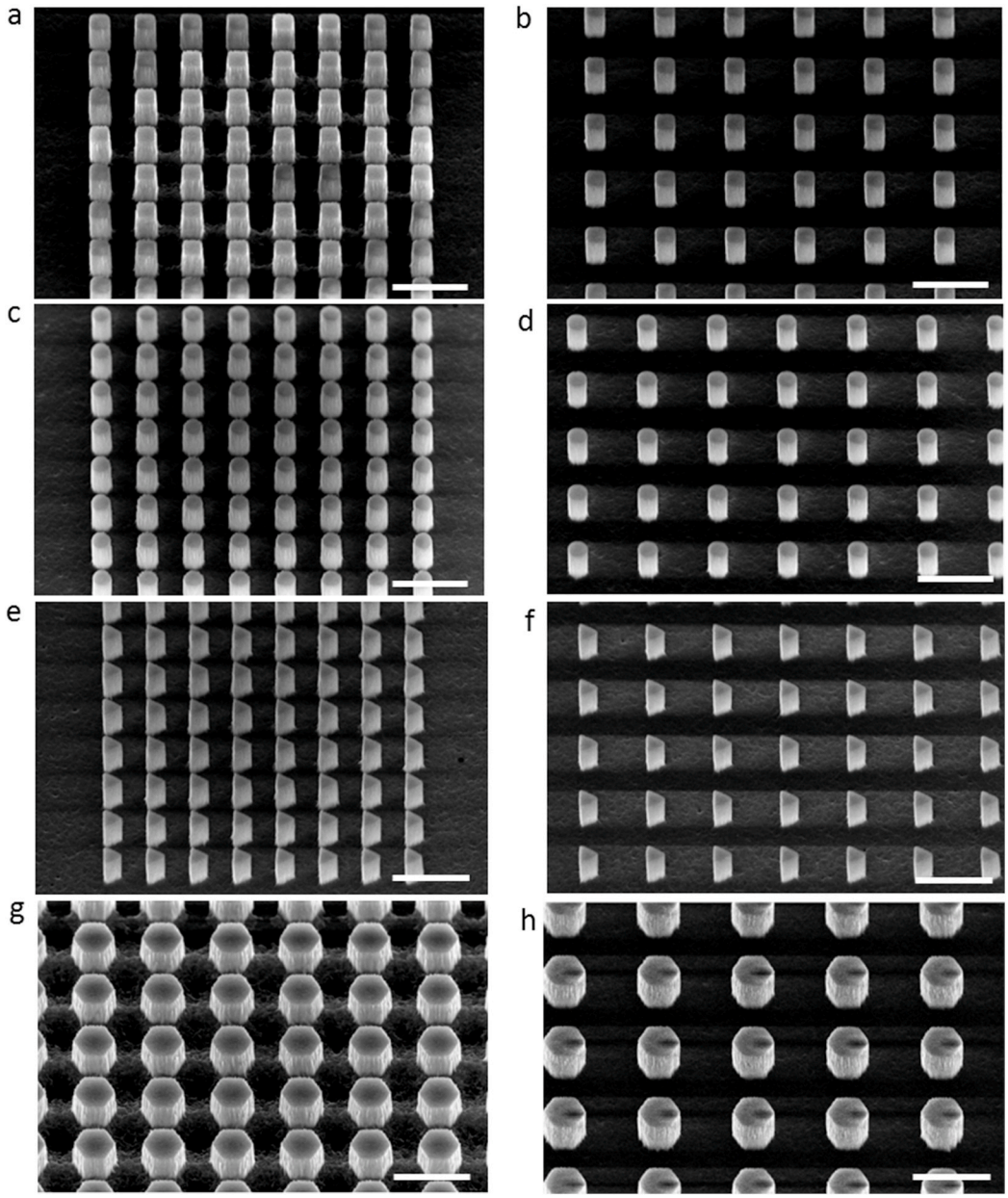

Fig. 4. Different pitches for Mo NP arrays with a pitch of 300 nm **(a), (c), (e), (g)** and of 600 nm **(b), (d), (f), (h).** As in Fig. 3 these NP exhibit square **(a), (b)**, circular **(c), (d),** triangular **(e), (f)** and hexagonal **(g), (h)** cross-sections respectively. For all arrays a 500 nm Mo layer is used for the NP fabrication. The scale bar is 1 μm.

critical point drying (CPD) together with SiO_2 as an adhesion layer is necessary to counteract the problems associated to the aged FOx resist. Fig. 5a and b displays the nanostructures fabricated with the modified resist recipe can be seen.

First of all, with modified recipe we are able to reproduce nanopillar structures with the desired etch profile, as shown in Fig. 5a for the case of NPs with square cross-sections.

Furthermore, we are able to fabricate nanopillars of Mo where the base is noticeably wider than the top, which will be referred to as nanocones in the following, and that are displayed in Fig. 5b. The fabrication of such Mo nanocones is achieved by slightly modifying the etching process. For the etching procedure of the straight sidewall structures, a Si carrier wafer is used where a thick layer of SiO_2 is deposited via LPCVD. Instead, for the nanocones etching procedure, a Si carrier wafer is used where both sides have a thick layer of SiO_2 thermally grown.

In both lithographic processes (leading to the square cross-section NP and the nanocones) we observed that the dosage needed to produce nanostructures of specific diameters varies with the size of these structures. Fig. 5c displays the dose required for specific dimensions and shapes of the resulting Mo NPs. In both cases, it is found that the smaller structures require a higher exposure. Additionally, in order to ensure straight sidewalls, it is necessary to avoid a too high platen power which could etch away the FOx resist before all the unexposed Mo metal is etched away. Fig. 5d indicates the etch rate as a function of platen power at fixed ICP power and gas flows. For the sub-150 nm structures, lower platen power results in the formation of straight sidewalls in the Mo metal. We note that the etch rate in the ICP-RIE system changed abruptly during the optimization process and Fig. 5d denotes the current etch rates for Mo in the Oxford Instruments PlasmaPro 100 Estrelas ICP-RIE system. A higher etch rate for the Mo NPs was found following the abrupt etch rate change. Decreasing the platen power led to recovering

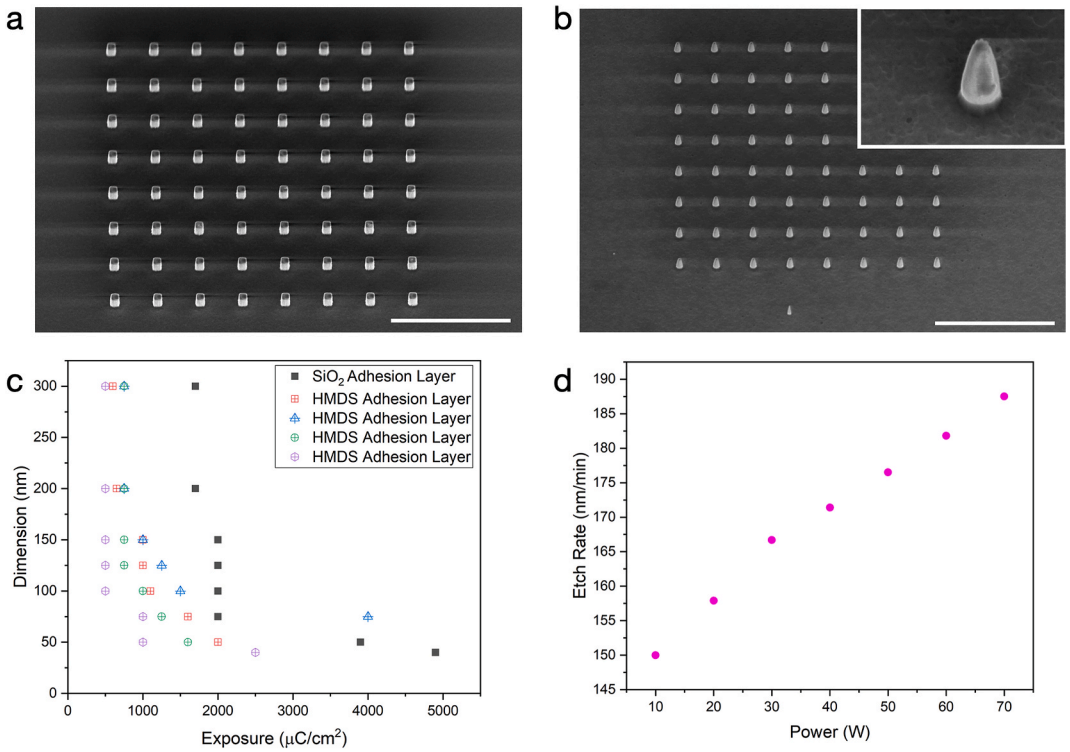

Fig. 5. **(a)** SEM images of the Mo NP array with square cross-sections fabricated with the modified resist recipe. **(b)** Same as **(a)** now for Mo nanocone arrays. Both in **(a)** and **(b)** the scale bar is 5 μm. **(c)** Dosage needed as function of the nanostructure dimensions. The shape of each marker is the same as the cross-section of the corresponding nanopillars. **(d)** Etch rate (in nm/min) as a function of the platen power at 1100 W ICP power.

the NPs with the desired etch profiles. The etch rate in ICP-RIE systems tend to drift over time, which could be a consequence of a change in the process chamber, *e.g.* Helium leakage into the process chamber, or using different clamping rings in the process chamber [39,40]. As of writing, the etch rates denoted in Fig. 5d have remained stable. Further research is necessary to understand the origin of the abrupt change in etch rate of the ICP-RIE system.

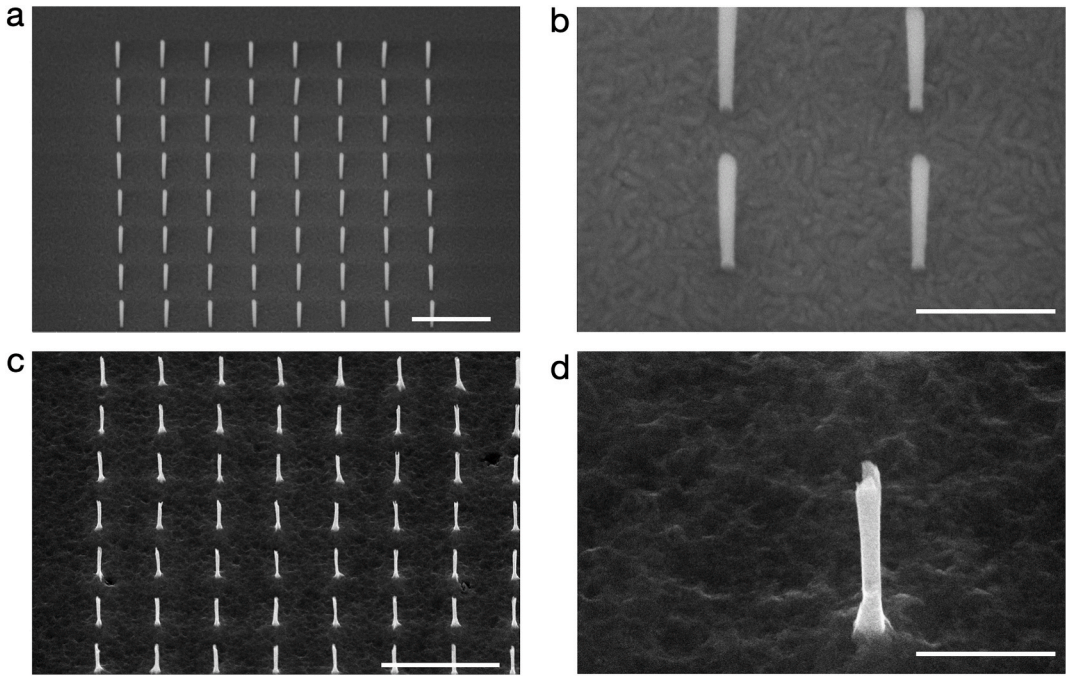

Fig. 6. (a)–(b) SEM images of 800 nm thick HSQ resist NP array. Diameters down to 40 nm with square cross-sections fabricated with the modified resist recipe. (c)–(d) Mo metal NPs fabricated with the unmodified resist process, with a length of 880 nm and width of 60 nm. The scale bar in (a) is 1 μm, and the scale bar in (c) is 2 μm. Both in (b) and (d) the scale bar is 400 nm.

3.2. High-aspect ratio Mo NPs

In Fig. 6 the limits of the modified and unmodified resist recipes and etching procedures can be seen. In Fig. 6a and b the HSQ resist NPs made with the modified resist recipe in a 800 nm thick HSQ layer are shown. Diameters down to 40 nm are achieved at relatively high exposures (~5300 μC/cm^2) with the modified HSQ resist recipe. For resist NP diameters below 100 nm a minimum of 100 nm pillar-to-pillar distance can be achieved with the modified resist recipe before overexposure becomes an issue. Fig. 6c and d displays square Mo NPs with a length of 880 nm and diameters down to 60 nm made with a HSQ resist mask of 600 nm using the unmodified recipe. For the Mo NP structures in Fig. 6c and d the HSQ resist was completely etched away during the cryogenic etching process, which can explain the loss of shape retention of the NP. For both the modified and unmodified resist recipes we note that for features below 75 nm in size the shape of the Mo NPs is not maintained after cryogenic etching.

The loss of shape for small diameters could be due to the very aggressive plasma parameters used. We have observed that the exposure needed for the HSQ resist for features greater than 100 nm tends to stay stable over the span of months, while the exposure required for sub-100 nm structures tends to increase as the HSQ resist ages, both for the modified and unmodified resist recipes.

4. Conclusions

In this work, we have demonstrated the feasibility of a novel strategy for the top-down large-scale fabrication of geometric arrays of Mo NPs with different cross-sectional shapes as well as of nanocones. Our approach is based on the combination of electron beam lithography and cryogenic deep-reactive ion etching, and makes possible a precise control on the shapes, lengths, diameters, and pitches of the resulting Mo NP arrays, which in all cases are characterized by well-defined smooth sidewalls.

The proposed top-down approach is not limited to the fabrication of nanopillars, since one can easily modify the shape of the etched molybdenum by changing the exposure design of the resist mask. In this respect, our method for the deep etching of structures in molybdenum could also be used to etch metals with similar etch chemistries. It is found that the limiting factor for large-aspect ratio of the NPs is the thickness of the resist mask, where the used FOx resist has a low selectivity during cryogenic reactive ion etching of the molybdenum. These results represent an attractive route towards the realization of high-density Mo NP arrays for applications from nanoelectronics to quantum sensing and hydrogen evolution reaction catalysis.

Declaration of competing interest

The authors declare that they have no known competing financial interests or personal relationships that could have appeared to influence the work reported in this paper.

Acknowledgements

S.C.-B. acknowledge financial support from the ERC through the Starting Grant “TESLA”, grant agreement no. 805021. L.M. acknowledges support from the Netherlands Organizational for Scientific Research (NWO) through the Topconsortia voor Kennis en Innovatie (TKI) program.

References

[1] M. Zach, K. Ng, R. Penner, Molybdenum nanowires by electrodeposition, Science 290 (2000) 5499.
[2] A. Kovic, A. Znidarsic, A. Jesih, A. Mrzel, M. Gaberscek, A. Hassanien, A novel facile synthesis and characterization of molybdenum nanowires, Nanoscale Res. Lett. 7 (2012) 567.
[3] J. Zhou, S. Deng, L. Gong, Y. Ding, J. Chen, J. Huang, J. Chen, N. Xu, Z.L. Wang, Growth of large-area aligned molybdenum nanowires by high temperature chemical vapour deposition: synthesis, growth mechanism, and device application, J. Phys. Chem. B 110 (2006) 10296.
[4] C.A. Spindt, I. Brodie, L. Humphrey, E.R. Westerberg, Physical properties of thin-film field emission cathodes with molybdenum cones, J. Appl. Phys. 47 (1976) 12.
[5] D. Dvorsek, M. Zumer, V. Nemanic, D. Mihailovic, Growth and field emission properties of vertically aliged molybdenum-sulfur-iodine nanowires on molybdenum and quartz substrates, J. Appl. Phys. 102 (2007) 114308.
[6] X. Zhang, F. Zhou, W. Pan, Y. Liang, R. Wang, General construction of molybdenum-based nanowire arrays of pH-universal hydrogen evolution electrocatalysis, Adv. Funct. Mater. 28 (2018) 43.
[7] K. Yeong, J. Thong, Field-emission properties of ultrathin 5 nm tungsten nanowire, J. Appl. Phys. 100 (2006) 114325.
[8] P.D. Christopher, K.K. Chan, J. Blum, Deep trench plasma etching of single crystal silicon using SF6/O2 gas mixtures, J. Vac. Sci. Technol. B: Microelectron. Nanometer Struct. Process. Measur. Phenom. 10 (1992) 1105.
[9] B.J.B. Tsengyou Syau, R.W. Hamaker, Reactive ion etching of silicon trenches using SF6/O2 gas mixtures, J. Electrochem. Soc. 138 (1991) 3076.
[10] B. Wua, A. Kumar, S. Pamarthy, High aspect ratio silicon etch: a review, J. Appl. Phys. 108 (2010), 051101.
[11] R. Legtenberg, H. Jansen, M.d. Boer, M. Elwenspoek, Anisotropic reactive ion etching of silicon using $SF_6/O_2/CHF_3$ gas mixtures, J. Electrochem. Soc. 142 (1995) 6.
[12] H. Janse, M.d. Boer, J. Burger, R. Legtenberg, M. Elwenspoek, The black silicon method II: the effect of mask material and loading on the reactive ion etching of deep silicon trenches, Microelectron. Eng. 27 (1995) 475.
[13] P.V. Antonov, M.R. Zuiddam, J.W.M. Frenken, Fabrication of high-aspect ratio silicon nanopillars for tribological experiments, J. Nanolithogr. MEMS, MOEMS 14 (2015), 044505.
[14] C. Fischer, J.W. Menezes, S.A. Moshkalev, C. Verissimo, A.R. Vaz, J.W. Swart, Fabrication of high-aspect ratio silicon nanopillars and nanocones using deep reactive ion etching, J. Vac. Sci. Technol. B: Microelectron. Nanometer Struct. Process. Measur. Phenom. 27 (2009) 2732.
[15] L.S. Golobokova, Y.V. Nastaushev, F.N. Dultsev, D.V. Gulyaev, A.B. Talochkin, A. V. Latyshev, Fabrication and optical properties of silicon nanopillars, J. Phys. Conf. 541 (2014), 012074.
[16] X.L. Han, G. Larrieu, P.F. Fazzini, E. Dubois, Realization of ultra dense arrays of vertical silicon nanowires with defect free surface and perfect anisotropy using a top-down approach, Microelectron. Eng. 88 (2011) 2622.
[17] S. Franssila, Introduction to Micro Fabrication, second ed., 2010, ISBN 978-0-470-74983-8.
[18] A.E. Grigorescu, C.W. Hagen, Resists for sub-20-nm electron beam lithography with a focus on HSQ: state of the art, Nanotechnology 20 (2009) 292001.
[19] Z. Zhang, H. Duan, Y. Wu, W. Zhou, C. Liu, Y. Tang, H. Li, Improving the adhesion of hydrogen silsequioxane (HSQ) onto various substrates for electron-beam lithography by surface chemical modification, Microelectron. Eng. 128 (2014) 59.
[20] M. Haffner, A. Haug, A. Heeren, M. Fleischer, H. Peisert, T. Chasse, D.P. Kern, Influence of temperature on HSQ electron-beam lithography, J. Vac. Sci. Technol. B: Microelectron. Nanometer Struct. Process. Measur. Phenom. 25 (2007) 2045.
[21] T.P. Chow, A.J. Steckl, Plasma etching of refractory gates for VLSI applications, J. Electrochem. Soc. 131 (1984) 2325.
[22] S. Ma, Y. Xia, Y. Wang, K. Ren, R. Luo, L. Song, X. Chen, J. Chen, Y. Jin, Fabrication and characterization of a tungsten microneedle array based on deep reactive ion etching technology, J. Vac. Sci. Technol. B 34 (2016), 052002.
[23] W.S. Pan, A.J. Steckl, Selective reactive ion etching of tungsten films in CHF_3 and other fluorinated gases, J. Vac. Sci. Technol. B 6 (1988) 1073.
[24] A. Picard, G. Turban, Plasma etching of refractory metals (W, Mo, Ta) and silicon in SF_6 and SF_6-O_2. An analysis of the reaction products, Plasma Chem. Plasma Process. 5 (1985) 4.
[25] S. Tachi, K. Tsujimoto, S. Okudaira, Low-temperature reactive ion etching and microwave plasma etching of silicon, Appl. Phys. Lett. 52 (1988) 616.
[26] N. Chekurov, K. Grigoras, A. Peltonen, S. Franssila, I. Tittonen, The fabrication of silicon nanostructures by local gallium implantation and cryogenic deep reactive ion etching, Nanotechnology 20 (2009) 6.
[27] H. Jansen, H. Gardeniers, M.d. Boer, M. Elwenspoek, J. Fluitman, A survey of the reaction ion etching of silicon in microtechnology, J. Micromech. Microeng. 6 (1995) 14.
[28] H.V. Jansen, M.J.d. Boer, S. Unnikrishnan, M.C. Louwerse, M.C. Elwenspoek, Black silicon method X: a review on high speed and selective plasma etching of silicon with profile control: an in-depth comparison between Bosch and cryostat DRIE processes as a roadmap to next generation equipment, J. Micromech. Microeng. 19 (2009), 033001.
[29] M.J.d. Boer, J.G.E. Gardeniers, H.V. Jansen, E. Smulders, M. Gilde, G. Roelofs, J. N. Sasserath, M. Elwenspoek, Guidelines for etching silicon MEMS structures using fluorine high-density plasmas at cryogenic temperatures, J. Microelectromech. Syst. 11 (2002) 4.
[30] S. Tachi, K. Tsujimoto, S. Arai, T. Kure, Low-temperature dry etching, J. Vac. Sci. Technol. 9 (1991) 796.
[31] K. Tsujimoto, S. Okudaira, S. Tachi, Low-temperature microwave plasma etching of crystalline silicon, Jpn. J. Appl. Phys. 30 (1991) 3319.
[32] A. Agarwal, Seasoning of plasma etching reactors: ion energy distributions to walls and real-time and run-to-run control strategies, J. Vac. Sci. Technol. 26 (2008) 498.
[33] H. Namatsu, Y. Takahashi, K. Yamazaki, T. Yamaguchi, M. Nagase, K. Kurihara, Three-dimensional siloxane resist for the formation of nanopatterns with minimum

linewidth fluctuations, J. Vac. Sci. Technol. B: Microelectron. Nanometer Struct. Process. Measur. Phenom. 16 (1998) 69.
[34] C.L. Frye, W.T. Collins, The oligomeric silsesquioxanes, (HSiO3/2)n, J. Am. Chem. Soc. 92 (1970) 19.
[35] T. Wahlbrink, D. Kupper, J. Bolten, M. Moller, M. Lemme, H. Kurz, Supercritical drying for high aspect-ratio HSQ nano-structures, Microelectron. Eng. 83 (2006) 1124.
[36] D.L. Goldfarb, J.J.d. Pablo, P.F. Nealey, J.P. Simons, W.M. Moreau, M. Angelopoulos, Aqueous-based photoresist drying using supercritical carbon dioxide to prevent pattern collapse, J. Vac. Sci. Technol. B: Microelectron. Nanometer Struct. Process. Measur. Phenom. 18 (2000) 3313.
[37] H. Namatsu, K. Yamazaki, K. Kurihara, Supercritical resist drying, J. Vac. Sci. Technol. B: Microelectron. Nanometer Struct. Process. Measur. Phenom. 18 (2000) 780.
[38] H. Namatsu, Supercritical drying for water-rinsed resist systems, J. Vac. Sci. Technol. B: Microelectron. Nanometer Struct. Process. Measur. Phenom. 18 (2000) 3308.
[39] I. Marinkovic, Optomechanical Devices in the Quantum Regime, 2019, ISBN 978-90-8593-401-1.
[40] J. Hill, Nonlinear Optics and Wavelength Translation via Cavity-Optomechanics, 2013, https://doi.org/10.7907/DKW6-TF64.